

# Wave interaction in photonic integrated circuits: Hybrid analytical / numerical coupled mode modeling

Manfred Hammer

Theoretical Electrical Engineering, University of Paderborn, Germany

## ABSTRACT

Typical optical integrated circuits combine elements, like straight and curved waveguides, or cavities, the simulation and design of which is well established through numerical eigenproblem-solvers. It remains to predict the interaction of these modes. We address this task by a "Hybrid" variant (HCMT) of Coupled Mode Theory. Using methods from finite-element numerics, the optical properties of a circuit are approximated by superpositions of eigen-solutions for its constituents, leading to quantitative, low-dimensional, and interpretable models in the frequency domain. Spectral scans are complemented by the direct computation of supermode properties (spectral positions and linewidths, coupling-induced phase shifts). This contribution outlines the theoretical background, and discusses briefly limitations and implementational details, with the help of an example of a 2-D coupled-resonator-optical-waveguide configuration.

**Keywords:** integrated optics, numerical / analytical modeling, coupled mode theory, optical micro-ring and micro-disk resonator circuits, whispering gallery resonances

## 1. INTRODUCTION

Approaches labeled "Coupled mode theory" (CMT) have some history in the field of modeling and simulation in integrated optics. One considers systems that can be described well in terms of the evolution of several, known, or easily computable, basis modes along a common propagation coordinate. A set of coupled differential equations is being established, taking mutual perturbations of the basis modes into account. Numerical means are employed where analytical solutions of these differential equations can not be obtained. We refer to [1–3] and to the textbooks [4–7] for overviews. Although mere phenomenological CMT models are frequently seen, where certain quantities ("coupling coefficients") are treated as free parameters, e.g. for fitting experimental data, here we focus on methods that intend to predict the optical electromagnetic fields from first principles, given structural and material properties, and an excitation wavelength.

As an example that can be expected to be treatable by a coupled-mode model, Figure 1 introduces a short 2-D coupled-resonator-optical-waveguide (CROW) configuration. Similar chains of evanescently coupled ring resonators have attracted recent interest, for interest in their time delay properties [8–10], but also as a means of channeling of optical power over the path of the resonators.

On the one hand, modeling microresonator-based circuits similar to Figure 1 with "conventional" coupled mode theory is more or less straightforward [11, 12], in 2-D [13] as well as in 3-D [14]. One specifies coupling regions around the points of closest approach of the straight and bend cores, and establishes coupled mode equations for these straight/bend and bend/bend couplers, here with a common propagation coordinate  $x$ . Due to the varying core distance, these need to be solved numerically, with the solutions embedded into a scattering-matrix model of the entire CROW structure. Special care has to be taken when extracting modal amplitudes [13], due to the non-orthogonality of the overlapping basis fields.

On the other hand, it appears decidedly unnatural to have to describe the propagation of the bend mode along the ring segment using the Cartesian coordinate of the straight core axis. In particular for small rings, with correspondingly larger extent of the exterior radiative part of the bend mode profiles, the coupler regions need to be large, covering a substantial portion of the rings, such that the exiting bend cores are not even remotely co-aligned with the straight channels.

We shall see that the method as discussed in this paper avoids these (perhaps slightly academic) complications. No common propagation coordinate is introduced, and, correspondingly, one has to abandon the notion of differential coupled

---

M. Hammer, Theoretical Electrical Engineering, University of Paderborn, Warburger Straße 100, 33098 Paderborn, Germany,  
Phone: ++49 (0)5251/60-3560, Fax: ++49 (0)5251/60-3524, E-mail: [manfred.hammer@uni-paderborn.de](mailto:manfred.hammer@uni-paderborn.de)

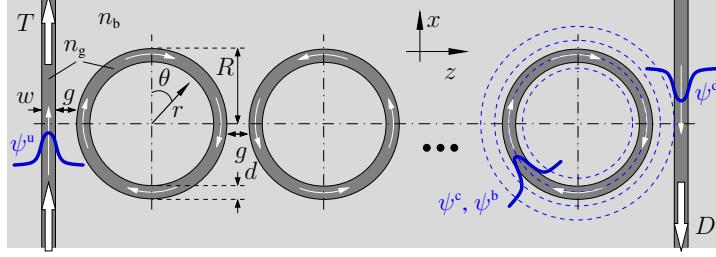


Figure 1. A sequence of microrings, coupled to two parallel bus waveguides, schematically. Modes  $\psi^u$  and  $\psi^d$  of the straight bus channels, propagating upward or downward in the positive or negative  $x$ -direction play a role, as well as clockwise or anticlockwise propagating bend modes  $\psi^b$  and whispering gallery resonances  $\psi^c$  associated with the individual cavity rings. Local coordinates  $r, \phi$  are introduced separately for each cavity. Parameters: refractive indices  $n_g = 1.5$  (cores, guiding regions),  $n_b = 1.0$  (background), core widths  $w = 0.6 \mu\text{m}$  (bus waveguides),  $d = 0.75 \mu\text{m}$  (rings), cavity radius  $R = 7.5 \mu\text{m}$  (outer rim), gap distances  $g = 0.3 \mu\text{m}$ , target vacuum wavelength  $\lambda \approx 1.56 \mu\text{m}$ .

mode equations. Numerical means, borrowed from the realm of finite elements (FEs), are employed instead. Concepts from analytical and numerical modelling play a role, hence the technique has been called ‘‘Hybrid analytical/numerical coupled mode theory’’ (HCMT). This paper gives a brief account of the approach as developed in Refs. [15–18], by means of the 2-D CROW configuration of Figure 1. We refer to [19] for a more detailed recent overview. Note that our list of HCMT examples includes structures such as a crossing of perpendicular waveguides [15], where ‘‘conventional’’ CMT would not be applicable, as well as ring resonator filters [17], where the HCMT results virtually coincide with ‘‘conventional’’ CMT data [13].

## 2. HYBRID COUPLED MODE THEORY

This concerns modelling in the frequency domain. A time dependence  $\sim \exp(i\omega t)$  of the time harmonic optical electric field  $\mathbf{E}$  and magnetic field  $\mathbf{H}$  is assumed, with the angular frequency  $\omega = kc$  specified by the vacuum wavelength  $\lambda = 2\pi/k$ , for vacuum wavenumber  $k$ , vacuum speed of light  $c$ , vacuum permittivity  $\epsilon_0$  and permeability  $\mu_0$ . We seek (approximate) solutions to the Maxwell curl equations

$$\nabla \times \mathbf{H} - i\omega\epsilon_0\epsilon\mathbf{E} = 0, \quad -\nabla \times \mathbf{E} - i\omega\mu_0\mathbf{H} = 0, \quad (1)$$

where, for linear, isotropic, and nonmagnetic dielectric media, the optical properties are given by the spatially dependent relative permittivity  $\epsilon = n^2$ , or refractive index  $n$ , respectively. Then the HCMT model requires a physically plausible ansatz, a ‘‘template’’, for the optical electromagnetic field as a starting point.

### 2.1 Field templates

As an example we consider the CROW structure of Figure 1, and we assume that the polarized modes  $\psi^u, \psi^d$  of the bus channels, and bend modes  $\psi_j^b$  supported by the curved cores of the cavity rings, are available, determined for some target wavelength. Given an excitation in the lower left port, one then expects the following behaviour. The upwards travelling mode in the left bus channel couples part of its power to a clockwise propagating bend mode in the leftmost ring. That mode in turn transfers part of its power to the anticlockwise propagating bend mode of the second cavity. Assuming an uneven number of rings, a fraction of the input power excites the downward propagating mode of the right bus core. We thus write a template for the overall electromagnetic field in the form

$$\begin{pmatrix} \mathbf{E} \\ \mathbf{H} \end{pmatrix}(x, z) = u(x)\psi^u(x, z) + d(x)\psi^d(x, z) + \sum_j b_j(\theta)\psi_j^b(r, \theta), \quad (2)$$

with as of yet unknown amplitudes  $u(x), d(x)$ , and  $b_j(\theta)$ , each a function of one variable. The formal relation  $r = r(x, z)$ ,  $\theta = \theta(x, z)$  between the local polar coordinates (a separate system for each cavity) and global Cartesian coordinates is to be understood implicitly for Eq. (2) to make sense, but will be taken into account explicitly only later.

The fields of the bus channels

$$\boldsymbol{\psi}^{\text{u,d}}(x, z) = \begin{pmatrix} \tilde{\mathbf{E}} \\ \tilde{\mathbf{H}} \end{pmatrix}^{\text{u,d}}(z) e^{\mp i\beta x} \quad (3)$$

cover the six electromagnetic components  $\tilde{\mathbf{E}}^{\text{u,d}}, \tilde{\mathbf{H}}^{\text{u,d}}$  of the mode profile, together with the exponential dependence on the propagation distance  $x$  with phase constants  $-\beta$  (upward propagation, left waveguide) and  $+\beta$  (downward propagation, right waveguide).

Waves travel around the (identical) cavities with indices  $j$  in the form of the clockwise or anticlockwise propagating bend modes [20]

$$\boldsymbol{\psi}_j^{\text{b}}(r, \theta) = \begin{pmatrix} \tilde{\mathbf{E}} \\ \tilde{\mathbf{H}} \end{pmatrix}_j^{\text{b}}(r) e^{\mp i\gamma R\theta}, \quad (4)$$

given in polar coordinates by the radial dependent bend mode profiles  $\tilde{\mathbf{E}}_j^{\text{b}}, \tilde{\mathbf{H}}_j^{\text{b}}$  and the complex angular propagation constant  $\gamma$ . Note that  $\gamma$  depends on the definition of the cavity radius  $R$  [11], here the outer rim of the rings. For non-integer  $\gamma R$ , the discontinuity of Eq. (4) at  $\theta = 0, 2\pi$  can be compensated [17, 19] through replacing  $\gamma$  by a real constant  $\kappa = \text{floor}(\text{Re}\gamma R + 1/2)/R$ , where  $\text{floor}(x)$  is the largest integer smaller than  $x$ . Any further variations in phase and amplitude, and also the bend mode losses, are then covered by the prospectively smooth amplitudes  $b_j(\theta)$  in Eq. (2).

Alternatively, one might decide to model the behaviour of the CROW structure in terms of the whispering gallery modes (WGMs) [18, 21] supported by the entire cavities. These are characterized — here in 2-D — by a radial order, by an integer angular mode number, and by a complex eigenfrequency. For excitation of the CROW with a given real frequency, one expects that only those WGMs with an eigenfrequency (real part) close to this excitation frequency contribute significantly to the solution. Clockwise and anticlockwise rotating fields, with respective positive or negative angular mode numbers, are selected in alternation for the rings in the sequence. One thus writes the template

$$\begin{pmatrix} \mathbf{E} \\ \mathbf{H} \end{pmatrix}(x, z) = u(x) \boldsymbol{\psi}^{\text{u}}(x, z) + d(x) \boldsymbol{\psi}^{\text{d}}(x, z) + \sum_j c_j \boldsymbol{\psi}_j^{\text{c}}(r, \theta). \quad (5)$$

Here the sum over  $j$  covers the separate cavities, as well as possible multiple WGMs of different radial or angular order for each cavity. The WGM fields  $\boldsymbol{\psi}_j^{\text{c}}(r, \theta) = (\tilde{\mathbf{E}}_j^{\text{c}}, \tilde{\mathbf{H}}_j^{\text{c}})(r, \theta)$  are meant to include both the electric and magnetic parts of the mode profiles. These are excited with as of yet unknown coefficients  $c_j$  (compare with the amplitude functions  $b_j(\theta)$  in Eq. (2)).

Note that the templates (2) and (5) represent merely the most simple type of unidirectional models. Straightforward extensions could concern bidirectional wave propagation, requiring additional terms with modes with propagation constants / angular mode numbers of opposite signs, or the inclusion of further modes of other / higher orders. Obviously, the templates decide which physical effects are covered by the model, and consequently, what can be expected from the approximate solutions. As an example, for the present circuits, losses due to the bend mode propagation along the ring, or alternatively, due to the radiative nature of the WGMs, are well taken into account, as becomes evident by the the spectra of Figures 2 and 3, where the dropped and transmitted power do not add up to one in general. Other loss mechanisms, e.g. radiation caused by the wave interaction in the regions where the cores come close, are not included in these models.

## 2.2 Amplitude discretization

What remains is to determine the functions  $u, d$ , and, depending on the template, the functions  $b_j$ , or the coefficients  $c_j$ . We continue directly with numerical means. After having identified a suitable interval of the  $x$ -axis, outside of which the amplitude  $u$  in the left bus channel can be expected to be constant,  $u$  is expanded into finite elements (FEs) as

$$u(x) = \sum_n u_n \alpha_n(x). \quad (6)$$

In the simplest case, the  $\alpha_n$  are the triangular functions associated with an equidistant 1-D first order FE discretization, with half infinite first and last elements. Explicit expressions, for the present context, are given in Refs. [15, 19]. An analogous discretization is applied to  $d(x)$ . The amplitudes  $b_j(\theta)$  of the bend modes are discretized on the interval  $\theta \in [0, 2\pi]$ , with the first and last element identified. The formal transformation to global Cartesian coordinates follows after the discretization.

After this step we are left with the task to find values for the now discrete coefficients  $u_n$ ,  $d_n$ , and either  $b_{j,n}$  or  $c_j$ . Using dots as wildcards for indices and arguments, the templates (2) or (5) now assume the generic form

$$\begin{pmatrix} \mathbf{E} \\ \mathbf{H} \end{pmatrix}(x, z) = \sum_k a_k \left( \alpha \cdot (\cdot) \psi \cdot (\cdot, \cdot) \right) =: \sum_k a_k \begin{pmatrix} \mathbf{E}_k \\ \mathbf{H}_k \end{pmatrix}(x, z).$$

Here the symbolic index  $k$  covers the summation over the channels of the bus waveguides, and the cavities, if applicable, over the possibly multiple modes in each channel or cavity, and the element indices of each separate FE discretization. The “modal elements”  $(\mathbf{E}_k, \mathbf{H}_k)$  combine the mode fields (3), (4), multiplied by the respective FE triangle functions, or they are directly the WGM profiles as introduced in Eq. (5). All coefficients are collected into one set of variables  $a_k \in \{u_n, d_n, b_{j,n}, c_j\}$ . Most of these are unknowns, but some represent the external influx: Given values of one for the coefficient of the first, half-infinite element of  $u$ , and zero for the last element in the discretization of  $d$ , specify a unit input in the lower left port, and zero input from the top in the right channel.

### 2.3 Algebraic procedure

Next we apply a projection procedure of Galerkin type to arrive at a linear system of equations for the  $a_k$ . A weak form of Eqs. (1) is obtained through multiplying by test fields  $\mathbf{E}'$  and  $\mathbf{H}'$ , and integrating the result. For reasons that become apparent in Section 2.5, we write it here such that the frequency parameter appears explicitly:

$$\iint \mathcal{A}(\mathbf{E}', \mathbf{H}'; \mathbf{E}, \mathbf{H}) \, dx \, dz - \omega \iint \mathcal{B}(\mathbf{E}', \mathbf{H}'; \mathbf{E}, \mathbf{H}) \, dx \, dz = 0 \quad \text{for all } \mathbf{E}', \mathbf{H}', \quad (7)$$

with

$$\mathcal{A}(\mathbf{E}', \mathbf{H}'; \mathbf{E}, \mathbf{H}) = (\mathbf{E}')^* \cdot (\nabla \times \mathbf{H}) - (\mathbf{H}')^* \cdot (\nabla \times \mathbf{E}) \quad (8)$$

and

$$\mathcal{B}(\mathbf{E}', \mathbf{H}'; \mathbf{E}, \mathbf{H}) = i\epsilon_0 \epsilon (\mathbf{E}')^* \cdot \mathbf{E} + i\mu_0 (\mathbf{H}')^* \cdot \mathbf{H}. \quad (9)$$

By inserting the general template (7) for  $\mathbf{E}, \mathbf{H}$ , and restricting the test fields to the modal elements  $\mathbf{E}_l, \mathbf{H}_l$ , one obtains the linear set of equations

$$\sum_k (A_{lk} - \omega B_{lk}) a_k = 0, \quad (10)$$

with “overlaps” of modal elements

$$A_{lk} = \iint \mathcal{A}(\mathbf{E}_l, \mathbf{H}_l; \mathbf{E}_k, \mathbf{H}_k) \, dx \, dz, \quad B_{lk} = \iint \mathcal{B}(\mathbf{E}_l, \mathbf{H}_l; \mathbf{E}_k, \mathbf{H}_k) \, dx \, dz, \quad K_{lk} = A_{lk} - \omega B_{lk}. \quad (11)$$

Further the coefficients  $\mathbf{a} = (a_k)$  are separated into unknowns  $\mathbf{u}$  and given quantities  $\mathbf{g}$ , and the matrix  $\mathbf{K} = (K_{lk})$  is rearranged accordingly. Then the system (10) can be given the form

$$\begin{pmatrix} K_{uu} & K_{ug} \\ K_{gu} & K_{gg} \end{pmatrix} \begin{pmatrix} \mathbf{u} \\ \mathbf{g} \end{pmatrix} = 0, \quad \text{or} \quad K_u \mathbf{u} = -K_g \mathbf{g} \quad \text{with} \quad K_u = \begin{pmatrix} K_{uu} \\ K_{gu} \end{pmatrix}, \quad K_g = \begin{pmatrix} K_{ug} \\ K_{gg} \end{pmatrix}. \quad (12)$$

Finally the unknowns in the — overdetermined — linear system of equations are determined in a least squares sense as a solution of

$$K_u^\dagger K_u \mathbf{u} = -K_u^\dagger K_g \mathbf{g}. \quad (13)$$

Here the symbol  $^\dagger$  denotes the adjoint. For a more detailed discussion of the procedure, and for an outline of an alternative true variational scheme, we refer to [15].

In line with the examples in Section 3, the above recipe has been given for a 2-D configuration with global Cartesian coordinates  $x$  and  $z$ . Extension to 3-D, then based on modes of straight and bend waveguides with 2-D cross sections, and resonance fields that depend on  $x, y$ , and  $z$ , would require merely to extend the expressions (7) and (11) to include integrals over the third spatial direction  $y$  as well.

## 2.4 Fast evaluation of spectral properties

Frequently, and in particular also for the present CROW structures, one is interested in the spectral response of a circuit. In principle, this requires to repeat the preceding procedures for a suitable sequence of excitation wavelengths. If only a narrow spectral range is of interest, and if material dispersion  $\epsilon(\omega)$ , if incorporated at all, is smooth in that range, one can expect that the properties of the basis modes, and consequently the values for their overlaps (11), vary but slowly with the vacuum wavelength. Any pronounced frequency dependence (in our case: resonance effects) must be attributed to the solution of the system (13). One might then consider to evaluate the modal element overlaps for a few representative wavelengths, and interpolate the respective matrices. Then only the solution of the moderately sized system (13) needs to be repeated to generate the spectral data. For further details we refer to [17]; in many cases we observed this an excellent approximation that speeds up the wavelength scans considerably.

## 2.5 Resonances of composite systems: Supermodes

For systems that exhibit resonant behaviour, rather than carrying out explicit spectral scans, one could be interested in a means to directly predict the resonance properties [18]. These are characterized by — prospectively complex — values  $\omega^s$  where the system

$$\nabla \times \mathbf{H} - i\omega^s \epsilon_0 \epsilon \mathbf{E} = 0, \quad -\nabla \times \mathbf{E} - i\omega^s \mu_0 \mathbf{H} = 0, \quad (14)$$

with boundary conditions of outgoing waves, becomes singular, i.e. permits nonzero solutions  $\mathbf{E}$ ,  $\mathbf{H}$ . For our specific configurations, we look for approximate solutions in the form of the templates (2), (5), now without any external input (the respective coefficients are set to zero). With the former frequency parameter  $\omega$  replaced by the unknown eigenfrequency  $\omega^s$ , one proceeds along the steps of Section 2.3 up to Eq. (10). Of Eq. (12) only the upper left quadrant remains relevant. After grouping the separate overlaps (11) into matrices  $\mathbf{A} = (A_{lk})$ ,  $\mathbf{B} = (B_{lk})$ , this sub-system can be given the form of a generalized eigenvalue problem:

$$\mathbf{A}_{uu} \mathbf{u} = \omega^s \mathbf{B}_{uu} \mathbf{u}. \quad (15)$$

Eq. (15) is to be solved for pairs of eigenvectors  $\mathbf{u}$  and eigenfrequencies  $\omega^s$ . One obtains a set of “supermodes”, each associated with a complex eigenfrequency  $\omega^s$ , quality factor  $Q = \text{Re } \omega^s / (2\text{Im } \omega^s)$ , resonance wavelength  $\lambda_r = 2\pi c / \text{Re } \omega^s$ , linewidth  $\Delta\lambda = \lambda_r / Q$ , and a supermode profile, which can be accessed by substituting the corresponding eigenvector into Eq. (7). For a template that includes the respective modes, this type of analysis takes into account power outlets through the bus waveguides. The resonance positions, Q-factors, and linewidths of the supermodes then describe the properties of the waves that the composite open cavity sends out through the access channels (cf. the respective statements in [22]).

## 3. NUMERICAL RESULTS

The present 2-D simulations rely on our C++ -implementation on the basis of quasi-analytical solvers for the modes of straight [23] and bend waveguides [24], and for the whispering gallery resonances of circular cavities. These basis fields can be considered “exact”, for all further numerical purposes.

Our list of benchmark examples includes straight parallel waveguides [15] (reference: analytical results), a waveguide crossing [15] (reference: a rigorous quasi-analytical solver), and configurations of micro-ring- and -disk resonators [17, 18] (comparison with conventional coupled mode theory [13] and with rigorous numerical results on the basis of finite elements or finite differences). The latter computations use the set of parameters of Figure 1, such that the confirmation should be, to some degree, transferable to the results shown below.

We consider the structure as introduced in Figure 1 with 9 cavities, for a spectral interval that is much narrower than the free spectral range ( $\approx 36$  nm, [18]) of one ring, around a target wavelength of  $1.56$   $\mu\text{m}$ . Here a single dielectric ring with the parameters of Figure 1 supports a whispering gallery mode WGM(0, 39) of fundamental radial order and angular order 39 with a resonance wavelength of  $1.56373$   $\mu\text{m}$ , a quality factor of  $1.1 \cdot 10^5$ , and a linewidth of  $1.4 \cdot 10^{-5}$   $\mu\text{m}$  [18].

### 3.1 CROW model based on bend modes

Our unidirectional HCMT model relies on the template (2). The fundamental bend mode supported by the curved cores of the cavities is included for each ring, with properly positioned origins and alternately clockwise and anticlockwise propagation directions. The amplitudes  $u$ ,  $d$  of the bus modes are discretized on an interval  $x \in [-10, 10]$   $\mu\text{m}$  with a stepsize of  $0.4$   $\mu\text{m}$ . For the bend mode amplitude of each ring, a FE discretization on the interval  $\theta \in [0, 2\pi]$  with a

stepsize of  $0.4 \mu\text{m}/R$  has been applied. This leads to a system (12) of dimension 1164, with two given values and 1162 unknowns, 1062 of which relate to the field of the composite 9-ring cavity. The procedure as outlined in Section 2.4 has been applied to evaluate the spectrum. Figure 2 summarizes the results.

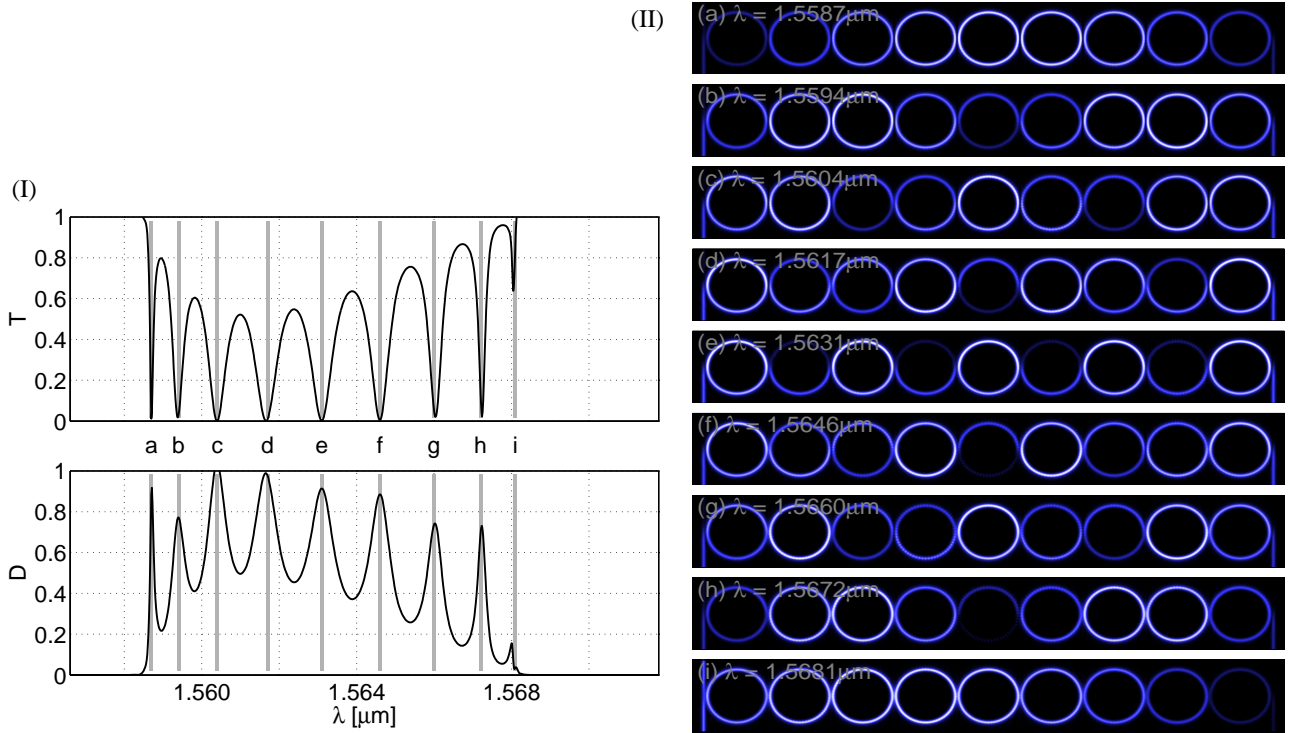


Figure 2. Bend-mode based HCMT model of a CROW structure of Figure 1 with 9 evanescently coupled rings. (I): relative transmitted  $T$  and dropped guided optical power  $D$ , as a function of the excitation wavelength  $\lambda$ . (II): field pattern associated with the resonances as indicated in (I); the plots show the absolute value of the principal electric component of the TE fields. [17]

Part (I) of Figure 2 shows the spectral transmission for a wavelength interval, that includes one resonance, i.e. one peak in the power drop  $D$  and simultaneous dip in the direct transmittance  $T$ , of a single ring device with comparable parameters [17]. For the present 9-ring CROW, that resonance splits into a series of 9 narrower peaks/dips, roughly at the position of former single-ring resonance. The spectral pattern of Figure 2(I) recurs with the free spectral range of the single ring [17]. Figure 2(II) shows the related resonant fields. One observes a systematic akin to standard Fourier harmonics, where “Nodes” are realized either by entire rings in an “off”-state, or as fields with opposite symmetry on both sides of a gap (not evident from the present plots). We shall see that these features can be explained by the simpler WGM model below.

### 3.2 CROW model based on whispering gallery resonances

As before, we carry out unidirectional HCMT simulations, now based on the template (5), where one WGM(0, 39), with alternating sense of rotation, is included for each ring. The amplitude functions of the bus waveguides are discretized by finite elements as in Section 3.1; for each ring one coefficient is introduced. The system (12) is of a dimension 111, with 109 actual unknowns. Now only 9 unknown coefficients relate to the field in the cavity. Figure 3 collects our results.

On the present narrow range around the WGM(0, 39)-resonance, the spectral response in part (I) of Figure 3 is qualitatively very similar to what is seen in Figure 2(I). Quantitative differences can be observed in the extremal levels of  $T$  and  $D$ , and in the wavelength positioning of the entire pattern. This pattern shifts to shorter wavelengths, if the simulations take into account further WGMs with nearby angular orders [18].

Furthermore we apply the procedures of Section 2.5 to the 9-ring CROW, leading to resonance wavelengths as indicated by the vertical lines in between the panels of Figure 3(I). If one uses a template (5) for the cavity rings only (the terms preceded by  $u$  and  $d$  are omitted), the HCMT supermode model, then with a system (15) of dimension 9, predicts a splitting

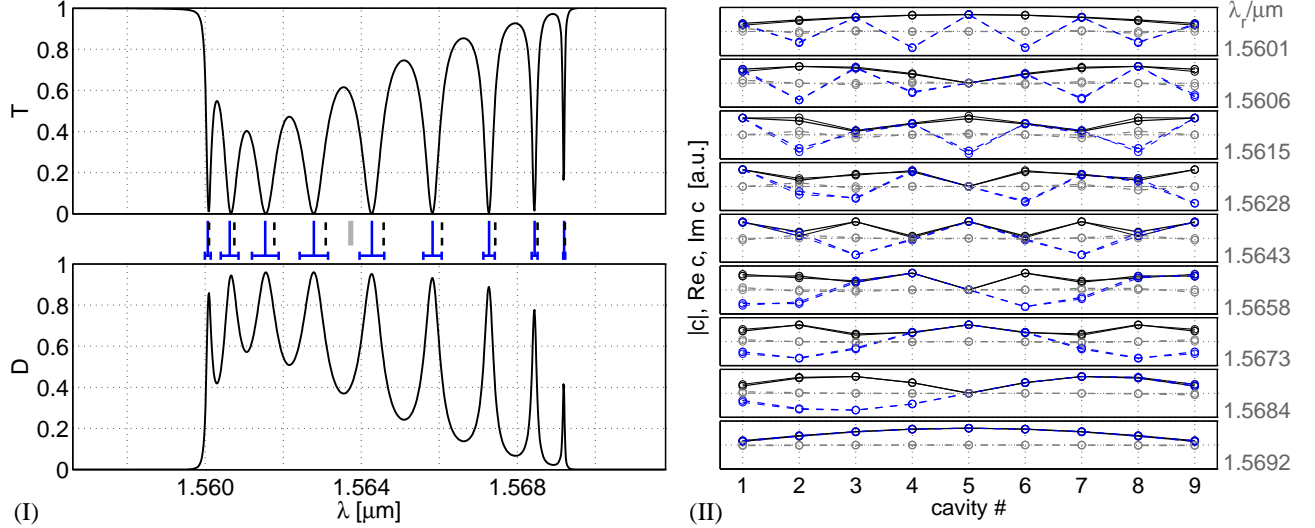


Figure 3. WGM-based HCMT model of a 9-ring CROW structure as in Figure 1. (I): Spectrum of the device, relative transmission  $T$  and power drop  $D$  as a function of the excitation wavelength  $\lambda$ . The markers in between the  $T$ - and  $D$ -panels show the positions of the resonance wavelength of one separate ring (single bold line, gray), of the supermode resonances for the series of rings without bus waveguides (dashed), and of the resonances of the complete system (continuous, here also the respective linewidths are shown). (II): Amplitude patterns for the supermodes of the system with bus waveguides (bold), and for the ring series only (thin lines, mostly shadowed). Real parts (dashed), imaginary parts (dash-dotted), and absolute values (continuous) of the coefficients assigned to the WGMs of neighboring cavities are connected to clarify the systematics. [18]

of the original resonance into a series of nine supermodes, positioned close to, but not quite at, the transmission resonances. An excellent approximation of the positions of the transmission extrema, and of their linewidths, is obtained, if the access waveguides are taken into account as well, i.e. by carrying out the HCMT supermode analysis with the full template (5).

Figure 3(II) shows the related “supermode profiles”, here the complex amplitudes assigned to the WGMs in the ring array. In good agreement with the fields of Figure 2(II), a systematic series of “harmonics” with a growing number of “nodes” is observed. The fundamental resonance, with the least “strained” profile (with the smallest variations in the real and imaginary parts of the WGM coefficients with respect to the cavity positions), appears at the longest resonance wavelength, that is at the lowest energy level.

#### 4. CONCLUDING REMARKS

Obviously, the HCMT approach as discussed above relies to a large extent on engineering intuition. For some given composite structure, the identification of a plausible field template, which necessarily cannot satisfy the Maxwell equations exactly, constitutes the major approximation. Still, once this template has been selected, one proceeds towards approximate solutions without any further heuristics.

The form of the general template (7) covers, in principle, also rigorous numerical discretizations of the optical fields. Hence one may regard this as a numerical finite element (FE) technique, but one with highly specialized, structure-adapted, largely global elements. Convergence can only be expected to lead to approximations in the form of the templates with *continuous* amplitude functions.

We have outlined the HCMT technique for the example of a specific resonator configuration, consisting of a series of identical cavity rings, excited through two parallel bus waveguides. Within certain limits, the semi-numerical model should be able to tackle similar CROW configurations, without principal restrictions on distances or positioning of elements, or on excitation conditions. HCMT models should thus be a convenient means to study other CROW-based circuits, like, e.g., bends in photonic molecules [25], defect-assisted CROWS [26], or tunable filters [27], from first principles, and including the access waveguides.

## ACKNOWLEDGMENTS

Financial support from the German Research Foundation (Deutsche Forschungsgemeinschaft DFG, projects HA 7314/1-1 and TRR 142) is gratefully acknowledged.

## REFERENCES

- [1] Chuang, S. L., “A coupled mode formulation by reciprocity and a variational principle,” *Journal of Lightwave Technology* **5**(1), 5–15 (1987).
- [2] Huang, W. P., “Coupled mode theory for optical waveguides: an overview,” *Journal of the Optical Society of America A* **11**(3), 963–983 (1994).
- [3] Hall, D. G. and Thompson, B. J., eds., [*Selected Papers on Coupled-Mode Theory in Guided-Wave Optics*], vol. MS 84 of *SPIE Milestone Series*, SPIE Optical Engineering Press, Bellingham, Washington USA (1993).
- [4] Vassallo, C., [*Optical Waveguide Concepts*], Elsevier, Amsterdam (1991).
- [5] Snyder, A. W. and Love, J. D., [*Optical Waveguide Theory*], Chapman and Hall, London, New York (1983).
- [6] März, R., [*Integrated Optics — Design and Modeling*], Artech House, Boston, London (1994).
- [7] Okamoto, K., [*Fundamentals of Optical Waveguides*], Academic Press, SanDiego (2000).
- [8] Yariv, A., Xu, Y., Lee, R. K., and Scherer, A., “Coupled-resonator optical waveguide: a proposal and analysis,” *Optics Letters* **24**(11), 711–713 (1999).
- [9] Little, B. E., Chu, S. T., Absil, P. P., Hryniewicz, J. V., Johnson, F. G., Seifert, F., Gill, D., Van, V., King, O., and Trakalo, M., “Very high-order microring resonator filters for WDM applications,” *IEEE Photonics Technology Letters* **16**(10), 2263–2265 (2004).
- [10] Canciamilla, A., Torregiani, M., Ferrari, C., Morichetti, F., De La Rue, R. M., Samarelli, A., Sorel, M., and Melloni, A., “Silicon coupled-ring resonator structures for slow light applications: potential, impairments and ultimate limits,” *Journal of Optics* **12**, 104008 (2010).
- [11] Hammer, M., Hiremath, K. R., and Stoffer, R., “Analytical approaches to the description of optical microresonator devices,” in [*Microresonators as building blocks for VLSI photonics*], Michelotti, F., Driessen, A., and Bertolotti, M., eds., *AIP conference proceedings* **709**, 48–71, American Institute of Physics, Melville, New York (2004).
- [12] Hiremath, K. R. and Hammer, M., “Circular integrated optical microresonators: Analytical methods and computational aspects,” in [*Photonic Microresonator Research and Applications*], Chremmos, I., Uzunoglu, N., and Schwelb, O., eds., *Springer Series in Optical Sciences, Vol. 156*, 29–59, Springer, London (2010).
- [13] Hiremath, K. R., Stoffer, R., and Hammer, M., “Modeling of circular integrated optical microresonators by 2-D frequency-domain coupled mode theory,” *Optics Communications* **257**(2), 277–297 (2006).
- [14] Stoffer, R., Hiremath, K. R., Hammer, M., Prkna, L., and Čtyroký, J., “Cylindrical integrated optical microresonators: Modeling by 3-D vectorial frequency domain coupled mode theory,” *Optics Communications* **256**(1–3), 46–67 (2005).
- [15] Hammer, M., “Hybrid analytical / numerical coupled-mode modeling of guided wave devices,” *Journal of Lightwave Technology* **25**(9), 2287–2298 (2007).
- [16] Hammer, M., “Chains of coupled square dielectric optical microcavities,” *Optical and Quantum Electronics* **40**(11–12), 821–835 (2009).
- [17] Hammer, M., “HCMT models of optical microring-resonator circuits,” *Journal of the Optical Society of America B* **27**(11), 2237–2246 (2010).
- [18] Franchimon, E., Hiremath, K., Stoffer, R., and Hammer, M., “Interaction of whispering gallery modes in integrated optical microring or -disk circuits: Hybrid CMT model,” *Journal of the Optical Society of America B* **30**(4), 1048–1057 (2013).
- [19] Hammer, M., “Guided wave interaction in photonic integrated circuits — a hybrid analytical / numerical approach to coupled mode theory,” in [*Recent Trends in Computational Photonics*], Agrawal, A., Benson, T., DeLaRue, R., and Wurtz, G., eds., *Springer Science*, 30 pp., Springer, London (2016, in preparation).
- [20] Hiremath, K. R., Hammer, M., Stoffer, R., Prkna, L., and Čtyroký, J., “Analytical approach to dielectric optical bent slab waveguides,” *Optical and Quantum Electronics* **37**(1-3), 37–61 (2005).
- [21] Prkna, L., Čtyroký, J., and Hubálek, M., “Ring microresonator as a photonic structure with complex eigenfrequency,” *Optical and Quantum Electronics* **36**(1/3), 259–269 (2004).
- [22] Popović, M. A., Manolatu, C., and Watts, M. R., “Coupling-induced resonance frequency shifts in coupled dielectric multi-cavity filters,” *Optics Express* **14**(3), 1208–1222 (2006).
- [23] Hammer, M., “METRIC — Mode expansion tools for 2D rectangular integrated optical circuits.” <http://metric.computational-photonics.eu/>.
- [24] Hiremath, K. R., “CIRCURS — Circular resonator simulator.” <http://home.iitj.ac.in/~k.r.hiremath/circurs/>.
- [25] Pishko, S. V., Sewell, P. D., Benson, T. M., and Boriskina, S. V., “Efficient analysis and design of low-loss whispering-gallery-mode coupled resonator optical waveguide bends,” *Journal of Lightwave Technology* **25**(9), 2487–2494 (2007).
- [26] Schwelb, O. and Chremmos, I., “Defect assisted coupled resonator optical waveguide: Weak perturbations,” *Optics Communications* **283**(19), 3686–3690 (2010).
- [27] Morichetti, F., Melloni, A., Breda, A., Canciamilla, A., Ferrari, C., and Martinelli, M., “A reconfigurable architecture for continuously variable optical slow-wave delay lines,” *Optics Express* **15**(25), 17273–17281 (2007).